Applied Catalysis B: Environmental 105 (2011) 77–85

Contents lists available at ScienceDirect

Applied Catalysis B: Environmental

journal homepage: www.elsevier.com/locate/apcatb

Photocatalytic hybrid nanocomposites of metal oxide nanoparticles enhanced towards the visible spectral range

Nihan Kosku Perkgoz*, Refik Sina Toru, Emre Unal, Mustafa Akin Sefunc, Sumeyra Tek, Evren Mutlugun, Ibrahim Murat Soganci, Huseyin Celiker, Gulsen Celiker, Hilmi Volkan Demir

UNAM – National Nanotechnology Research Center, Institute of Materials Science and Nanotechnology, Department of Physics, Department of Electrical and Electronics Engineering, and Materials Science and Nanotechnology (MSN) Program, Bilkent University, Ankara, 06800, Turkey

ARTICLE INFO

Article history:
Received 7 October 2010
Received in revised form 25 February 2011
Accepted 30 March 2011
Available online 13 April 2011

Keywords:
Immobilized nanoparticles
Nanocomposite films
Titanium dioxide
Zinc oxide
Photocatalytic activity
Optical characterization

ABSTRACT

We propose and demonstrate photocatalytic hybrid nanocomposites that co-integrate TiO_2 and ZnO nanoparticles in the same host resin to substantially enhance their combined photocatalytic activity in the near-UV and visible spectral ranges, where the intrinsic photocatalytic activity of TiO_2 nanoparticles or that of ZnO nanoparticles is individually considerably weak. For a comparative study, by embedding TiO_2 nanoparticles of ca. 6 nm and ZnO nanoparticles of ca. 40 nm in the sol–gel matrix of acrylic resin, we make thin film coatings of TiO_2–ZnO nanoparticles (combination of TiO_2 and ZnO, each with a mass ratio of 8.5%), as well as the composite films of TiO_2 nanoparticles alone (17.0%), and ZnO nanoparticles alone (17.0%), and a negative control group with no nanoparticles. For all of these thin films coated on polyvinyl chloride (PVC) polyester, we experimentally study photocatalytic activity and systematically measure spectral degradation (recovery obtained by photocatalytic reactions). This spectral characterization exhibits photodegradation levels of the contaminant at different excitation wavelengths (in the range of 310–469 nm) to distinguish different parts of optical spectrum where TiO_2 and ZnO nanoparticles are individually and concurrently active. We observe that the photocatalytic activity is significantly improved towards the visible range with the use of TiO_2–ZnO combination compared to the individual cases. Particularly for the excitation wavelengths of photochemical reactions longer than 400 nm, where the negative control group and ZnO nanoparticles alone yield no observable photodegradation level and TiO_2 nanoparticles alone lead to a low photodegradation level of 14%, the synergic combination of TiO_2–ZnO nanoparticles achieves a photodegradation level as high as 30%. Investigating their scanning electron microscopy (SEM), X-ray diffraction (XRD), and high resolution transmission electron microscopy (HRTEM), we present evidence of the heterostructure, crystallography, and chemical bonding states for the hybrid TiO_2–ZnO nanocomposite films, in comparison to the films of only TiO_2 nanoparticles, only ZnO nanoparticles, and no nanoparticles.

1. Introduction

Metal oxide nanoparticles have recently attracted worldwide attention for their superior photocatalytic properties. Such photocatalytic nanoparticles find a wide range of important environmental applications including self-decontamination of large areas (both indoors and outdoors) by decomposing organic compounds and viral, bacterial, and fungal species adsorbed on the surface and also reduction of air pollution by decreasing NO_x and CO_x amounts in air [1,2]. In operation, the range of optical spectrum where these photocatalysts become active is of fundamental importance, especially when their optical excitation mainly relies on sunlight. In general, the metal oxide nanoparticles are not photocatalytically excited in the visible range of solar spectrum, as they are typically made of wide bandgap semiconductors, e.g., TiO_2 and ZnO. The performance of such metal oxide semiconductor nanoparticles depends on the process of optical absorption of incident photons (with sufficient photon energy, typically falling into the UV range) and subsequent photogeneration of electron and hole pairs (which exhibit dissimilar parity in their respective conduction and valence bands, leading to low recombination rates) [2]. With longer lifetimes, these photogenerated electron–hole pairs diffuse to the nanoparticle surface before recombination to initiate a chain of photochemical reactions. Thus, to achieve high photocatalytic activity under solar illumination, photocatalyst semiconductors need to feature narrower bandgap matching the solar spectrum. However, this undesirably reduces photoactivity [3]. Therefore, there is a fundamental trade-off between the photochemical reac-

* Corresponding author at: UNAM – National Nanotechnology Research Center, Institute of Materials Science and Nanotechnology, Department of Physics, Bilkent University, Ankara 06800, Turkey. Tel.: +90 312 290 1021; fax: +90 312 290 1123.
E-mail addresses: kosku@bilkent.edu.tr, volkan@bilkent.edu.tr (N.K. Perkgoz).

0926-3373/$ – see front matter © 2011 Elsevier B.V. All rights reserved.
doi:10.1016/j.apcatb.2011.03.037

tions at the longer wavelengths and the level of photoactivity. As a result, it has been very challenging to obtain photocatalysts with the capability of efficient photocatalytic activation in the visible range.

Various approaches have been reported to modify electronic structure of metal oxides and enhance photocatalytic efficiency under sunlight. One of the reported techniques is to use selective doping to control properties of metal oxides [4]. For this, nitrogen has been found to be beneficial to allow for bandgap narrowing and absorption enhancement [5]. Boron doping [6] and carbon doping [7] have also been reported to facilitate increased absorption of visible light. Another promising solution reported for higher photocatalytic efficiency under daylight is to mix two or more different kinds of metals into oxide systems. Such systems are useful for promoting the separation of electron hole pairs and keeping reduction and oxidation reactions at two different reaction sites [8]. Different hybrid metal oxides such as Co_3O_4–$BiVO_4$ [9], Cu_2O–TiO_2 [10], RuO_2–WO_3 [11], TiO_2–ZnO [12–17] have been reported for enhanced visible response.

In the literature, to date, although there is considerable amount of research work reported for the investigation of photocatalytic activation of TiO_2 nanoparticles alone and ZnO nanoparticles alone, which are separately immobilized in thin films (e.g. [2,18]), and there are also prior works analyzing ZnO–TiO_2 systems that show improved separation of the photogenerated charge carriers [12–17], there is no previous report on a systematic optical excitation study of combined TiO_2 and ZnO nanoparticles that are employed together in a single composite film for enhanced photocatalytic activity at longer wavelengths for large area applications.

In this paper, different than prior works of our group [19–22] and others [12–17], to address this need for enhanced photocatalysis in the solid film towards the visible, we present optical study of photocatalytic hybrid nanocomposites that co-integrate TiO_2 and ZnO nanoparticles in the same resin host to substantially enhance their combined photocatalytic activity in the near-UV and visible spectral ranges, where the intrinsic photocatalytic activity of TiO_2 nanoparticles or that of ZnO nanoparticles is individually considerably weak. Normally immobilization reduces effective catalyst surface and photocatalytic efficiency [23,24]. This is due to the fact that the photo-induced carrier transfer takes place at the interface of the photocatalyst and the adsorbed material [25]. To recover this severely decreased efficiency as a result of the immobilization, nanostructured semiconductors can be used to increase their surface-to-volume ratio [18]. In our work, we used nanostructured semiconductors (TiO_2 of ca. 6 nm in size and ZnO of ca. 40 nm in size) with their high surface-to-volume ratios embedded in a three-dimensional (3-D) acrylic matrix, which conveniently provides a suitable host for a homogenous distribution of the metal oxides and reduces aggregates.

In this methodology, integration of nano-sized particles into the sol–gel matrix does not only provide high photocatalytic activity but also enables a highly dispersed, non-agglomerated nanoparticle material system with high surface roughness, increased surface hydrofobicity and decreased photodegradation of the host material. Such increased surface roughness, followed by hydrophobization, was also previously studied by different groups for different purposes, for example, for textile applications [26]. Such sol–gel process offers advantages including high purity, good uniformity of the film microstructure, low-temperature synthesis, and easily controlled reaction conditions [24]. Therefore, in this study, we obtain comparatively high photocatalytic activities of metal oxide nanoparticles embedded in sol–gel in spite of the fact that the particles are immobilized.

In our previous work, we investigated optical spectral response of only TiO_2 nanoparticles [19,20] and only ZnO nanoparticles [21,22] separately immobilized in sol–gel networks. We showed the size effect for TiO_2 nanoparticles by comparing their photocatalytic performance [19]. In this present work, unlike our previous studies, we embedded both TiO_2 and ZnO nanoparticles in the same resin for an enhanced photocatalytic activity towards the visible spectral range. Different from other research works, here we perform optical spectral excitation characterization of TiO_2 and ZnO nanoparticles combined in a single thin film, which is achieved in a simple and low cost method, to show different parts of the optical spectrum where these photocatalysts become active when together.

For the composite film, we developed acrylic resin for co-integration of TiO_2 and ZnO nanoparticles in its 3-D matrix. Hybrid organic–inorganic material formation via sol–gel route prevented degradation of the host resin by highly active photocatalytic nanoparticles. Therefore, during our photochemical reaction experiments, we observed the photocatalytic activity that stems from the degradation of contaminant methylene blue with the use of nanoparticles. In the literature, several methods that incorporate various metal oxides in the layered compounds for nanocomposite films were reported; using these, higher photocatalytic activities compared to unsupported photocatalysts were obtained [3]. However, these previous experiments do not show the optical spectral range over which the enhancement occurs. Such nanocomposites formed using various techniques have been mostly activated with direct sunlight [27], with a UV source that includes all UV wavelengths [28], or at a single activation wavelength [29]. But there is no complete spectral investigation of optical activation efficiency that shows where the enhancement contribution comes spectrally from. Using our integrated TiO_2–ZnO nanocomposite films, here we illustrate the enhancement of the photocatalytic activity achieved as a function of the activation wavelength in the spectral ranges of near-UV and visible. This renders critically important for outdoor (and some indoor) applications that rely mostly on the sunlight, as these spectral ranges of near-UV and visible are stronger in the solar spectrum compared to the deeper UV ranges, commonly required for conventional photocatalysis. Nanocomposite metal oxides offer a strong potential to be used in different large-area environmental applications including wide-scale self-decontamination (both indoors and outdoors) by decomposing organic compounds and viral, bacterial, and fungal species adsorbed on the surface. However, towards this end, their photocatalytic activity in the visible range still needs to be improved and practical production methods need to be explored, especially considering the fact that photocatalytic reactions have thus far been studied mostly in aqueous environment. In this paper, to address these issues, we propose and demonstrate photocatalytic hybrid nanocomposite films that employ TiO_2 and ZnO nanoparticles in the same host resin to substantially enhance their combined photocatalytic activity in the near-UV and visible spectral ranges. Here the novelty of this work comes from the simple approach of co-integrating TiO_2 and ZnO nanoparticles into a single nanocomposite structure to surpass their individual intrinsic photocatalytic activities in the near-UV and visible. In this paper, as a result, the contribution of this work is two folds: First we systematically investigate and demonstrate that photocatalytic reaction efficiency can be increased in solid form by using hybrid nanocomposites of TiO_2 and ZnO nanoparticles incorporated in the same acrylic sol–gel resin for large-area photocatalytic applications, which can potentially lead to wide-scale self-cleaning applications (because such thin films can easily be formed even by spraying). Second, we spectrally characterize photodegradation levels of the contaminant at a series of excitation wavelengths from the visible to UV to distinguish the activation range of optical spectrum, which has been previously missing in the prior literature. In this work, this systematic optical excitation study of TiO_2 and ZnO nanoparticles combined together in a single composite film demonstrated hybrid photocatalytic nanocompos-

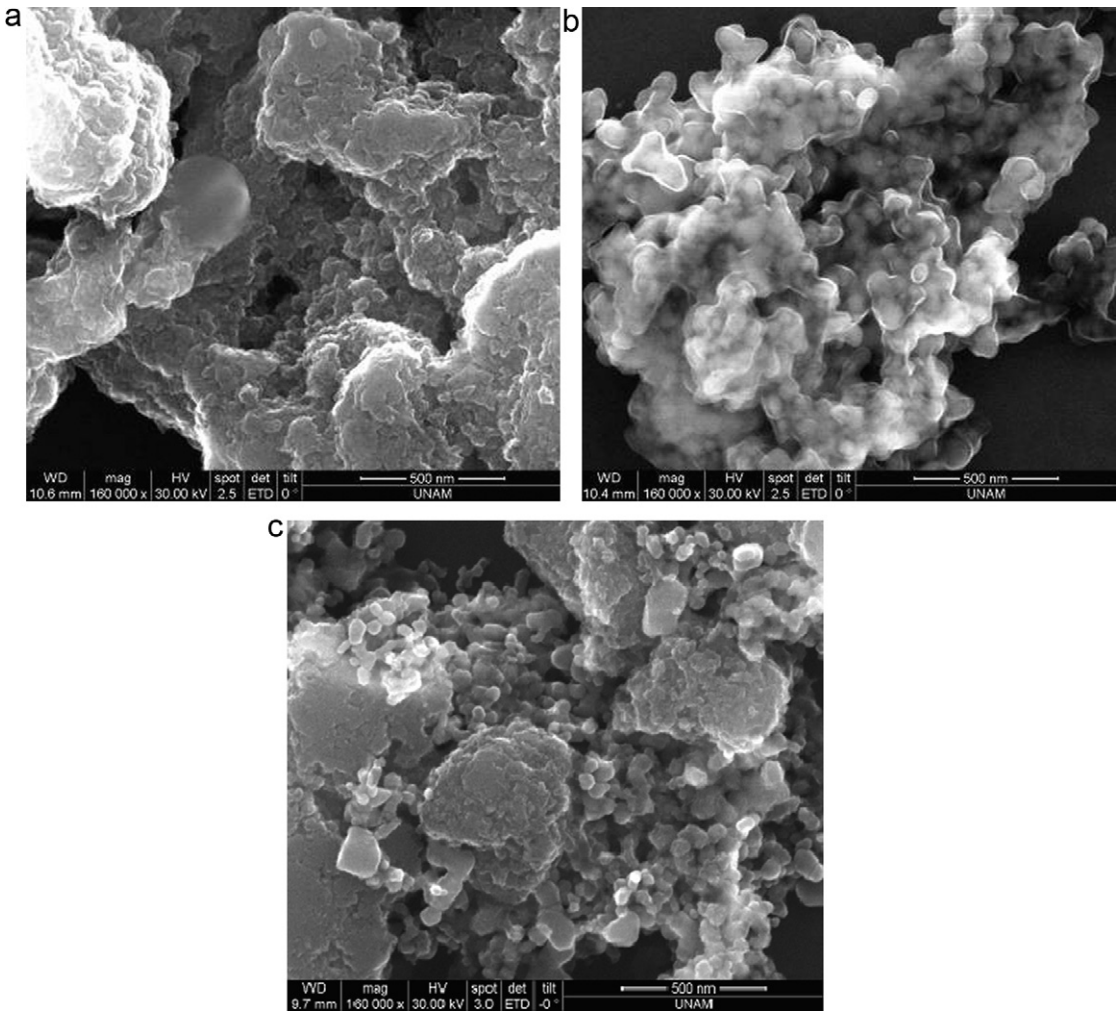

Fig. 1. Scanning electron microscopy (SEM) images of nanocomposite thin films of (a) TiO_2 nanoparticles alone, (b) ZnO nanoparticles alone and (c) combination of both TiO_2–ZnO nanoparticles on Si (1 0 0). In all of these SEM images, the scale bar is 500 nm.

ites with substantially enhanced optical activity in solid form at longer wavelengths. This hybrid nanocomposite film approach, which is simple and compatible with mass production, is expected to contribute to combating various forms of environmental pollution.

2. Experimental

In this work, we formed three different sets of nanoparticle composite films, each with a ~10 μm thickness: (1) with the combination of TiO_2–ZnO (8.5 mass% of TiO_2 and 8.5 mass% of ZnO; a total of 17.0% from both nanoparticles), (2) only with TiO_2 of 17.0%, and (3) only with ZnO of 17.0% in the films. For all three types of these nanocomposite material systems, the associated nanoparticles were integrated into identical acrylic resin on polyvinyl chloride (PVC) coated polyester substrates for optical characterization. We prepared the silicate matrix using the widely known sol–gel technique based on hydrolysis and condensation reactions of two types of silicon alkoxides, and controlled their rates by HCl catalyst, as shown below, where R is an alkyl group. As well known, hydrolysis provides reactive silanol groups and condensation leads to the formation of bridging oxygen.

$$Si\text{–}(OR)_4 + H_2O \rightarrow (RO)_3SiOH + ROH\{\text{hydrolysis}\}$$

$$2(RO)_3SiOH \rightarrow (RO)_3Si\text{–}O\text{–}Si(OR)_3 + H_2O\{\text{condensation}\}$$

$$(RO)_4Si + (RO)_3SiOH \rightarrow (RO)_3Si\text{–}O\text{–}Si(OR)_3 + ROH$$

For the reaction medium of the sol–gel reaction, we used ethyl alcohol and isopropyl alcohol. We set the starting reaction temperature to 50 °C. We modified our metal oxides within the sol–gel in situ while we added acrylic and methacrylic esters to the system. During the modification of metal oxides and acrylic resin synthesis, we increased the reaction temperature to 85 °C. After the completion of monomer conversion, we finally decreased the reaction temperature to the room temperature and further mixed the metal oxides in the sol–gel at least for 2 h at a rate of 3500 rpm. Hydrolysis and condensation rates of silicon alkoxides are enhanced by acid or base catalysis. We used the same procedure for all of our metal oxide types (only ZnO, only TiO_2, and their combination). As a result of the integration, we obtained nanocomposite materials with their nanoparticles dispersed more uniformly than mere mechanical blending. We varied and investigated the ratios of sol–gel to metal oxides and metal oxide to acrylic resin in terms of their photocatalytic performance and stability. The optimum ratios were found to be 50% for the metal oxide modification and 17% for the total metal oxide content. We assessed the structure and morphology of the nanocomposites by using scanning electron microscopy (SEM) by drop casting the nanocomposite sol–gel matrix on Si (1 0 0)

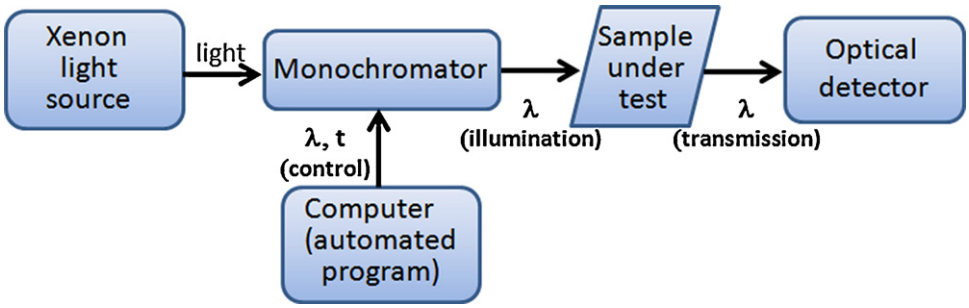

Fig. 2. Our photocatalytic degradation measurement set-up.

substrate provided in Fig. 1a–c. SEM images exhibit immobilization of only TiO_2 nanoparticles, only ZnO nanoparticles and their combination in their respective samples. Fig. 1c shows that integrating titania and ZnO particles together in the sol–gel matrix provides a comparatively more porous structure and thus leads to effectively a larger activation area for enhanced photocatalytic reactions.

As shown in Fig. 2, for our photocatalytic degradation measurements, we used a monochromator (CM 110 Spectral Products) and a Xenon light source to spectrally activate our thin films in the UV and the visible wavelength range, and to perform transmission measurements using Newport powermeter. The measurements were computerized and automated by in-house developed Labview programs. The components such as the monochromator and powermeter were controlled via GPIB (General Purpose Interface Bus) interfaces. Optical analysis of the photocatalytic recovery was carried out through a standard process of contaminating our samples and then activating them under illumination of a monochromatic light at a specified wavelength (λ). After each controlled activation period, the optical transmission measurement of the activated sample was taken for optical recovery analyses.

3. Results and discussion

We applied the nanocomposites in the sol–gel matrix on flat PVC coated polyester substrates through spray coating method. We carefully adjusted the spray coating to obtain the same thin film thickness (~10 μm) for all of our dry films. Also, our electron dispersion spectroscopy (EDS) characterizations of these samples confirm that only TiO_2 nanocomposite samples include only Ti (thus only TiO_2 nanoparticles) but no Zn (thus no ZnO nanoparticles), that only ZnO nanocomposite samples include only Zn (thus only ZnO nanoparticles) but no Ti (thus no TiO_2 nanoparticles), and that TiO_2–ZnO samples include both Ti and Zn (thus both TiO_2 and ZnO nanoparticles).

To obtain phase identification of these hybrid nanocomposites, Fig. 3 shows normalized XRD patterns of only TiO_2, only ZnO and TiO_2–ZnO nanoparticle thin films on Si substrates. We attained the diffraction peaks of TiO_2 and ZnO by using the standard spectra (JCPDS reference codes: 01-070-6826 and 00-001-1136, respectively). For only TiO_2 integrated films, XRD patterns exhibit diffraction peaks at ~25° (1 0 1) and ~48° (2 0 0) indicative of the anatase phase. The patterns exhibit broad peaks due the small-size TiO_2 nanoparticles. We calculate the average grain size to be ~6 nm by applying the Debye–Sherrer formula, which is in agreement with the size measured by TEM. In the case of only ZnO integrated films, XRD patterns show diffraction peaks at ~36° (1 0 1) and ~31° (1 0 0) specifying zincite-hexagonal phase. We calculate the average grain size to be ~40 nm by applying the Debye–Scherrer formula. The peaks are in conformity with the standard spectrum. The broad peaks at ~19° show the silica phase in the sol–gel matrix. The patterns illustrate that there is no chemical change when ZnO and TiO_2 nanoparticles are integrated in the sol–gel matrix and the interaction between TiO_2 and ZnO in TiO_2–ZnO films is suggested to be in the electronic states due to the charge transfer decreasing the recombination rate of the generated electron–hole pairs.

To investigate the composition, structure and morphology of the photocatalytic hybrid TiO_2–ZnO nanocomposites, in Fig. 4, we present the lattice image taken by transmission electron microscopy (TEM) using Tecnai G2 F3 electron microscope with a 200 kV acceleration voltage. As shown in Fig. 4a and b, we observe that the grain size of TiO_2 and ZnO nanoparticles is about 6 and 40 nm, respectively. The results illustrate that the grains are in crystalline phase and the crystallite sizes are in agreement with the calculated grain sizes from the XRD patterns as it was shown in Fig. 3.

For optical characterizations, we used a Xenon light source and a monochromator to activate our contaminated samples using monochromatic light at 16 different activation wavelengths tuned from 310 nm to 469 nm. We employed the standard industrial contaminant methylene blue for contamination by drop casting method. We optically characterized the photodegradation of the contaminant via its oxidization with the active radicals generated on metal oxide surfaces as a result of optical activation. In previous research works, e.g. [30], bleaching of methylene blue by UV-irradiated TiO_2 was also used. It was shown that bleaching cannot be due to a simple reduction of methylene blue to its leuco form but instead it had to be through a decomposition process. In our experiments, we used the activation power in the range of tens to hundreds of microwatts (which is sufficient to activate photochemical reactions but not to initiate direct photolysis for our

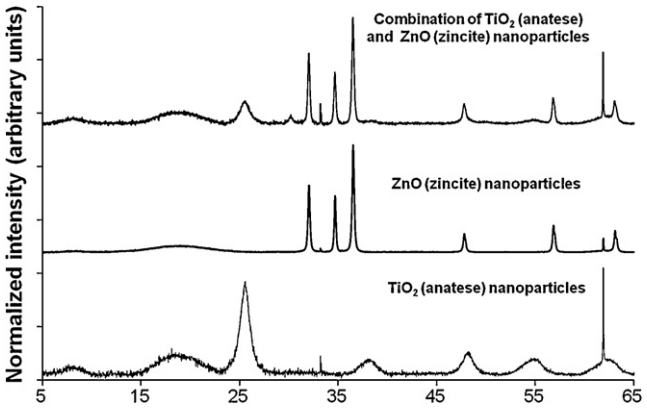

Fig. 3. Normalized XRD patterns of only TiO_2, only ZnO and TiO_2–ZnO nanoparticles immobilized in nanocomposite thin films.

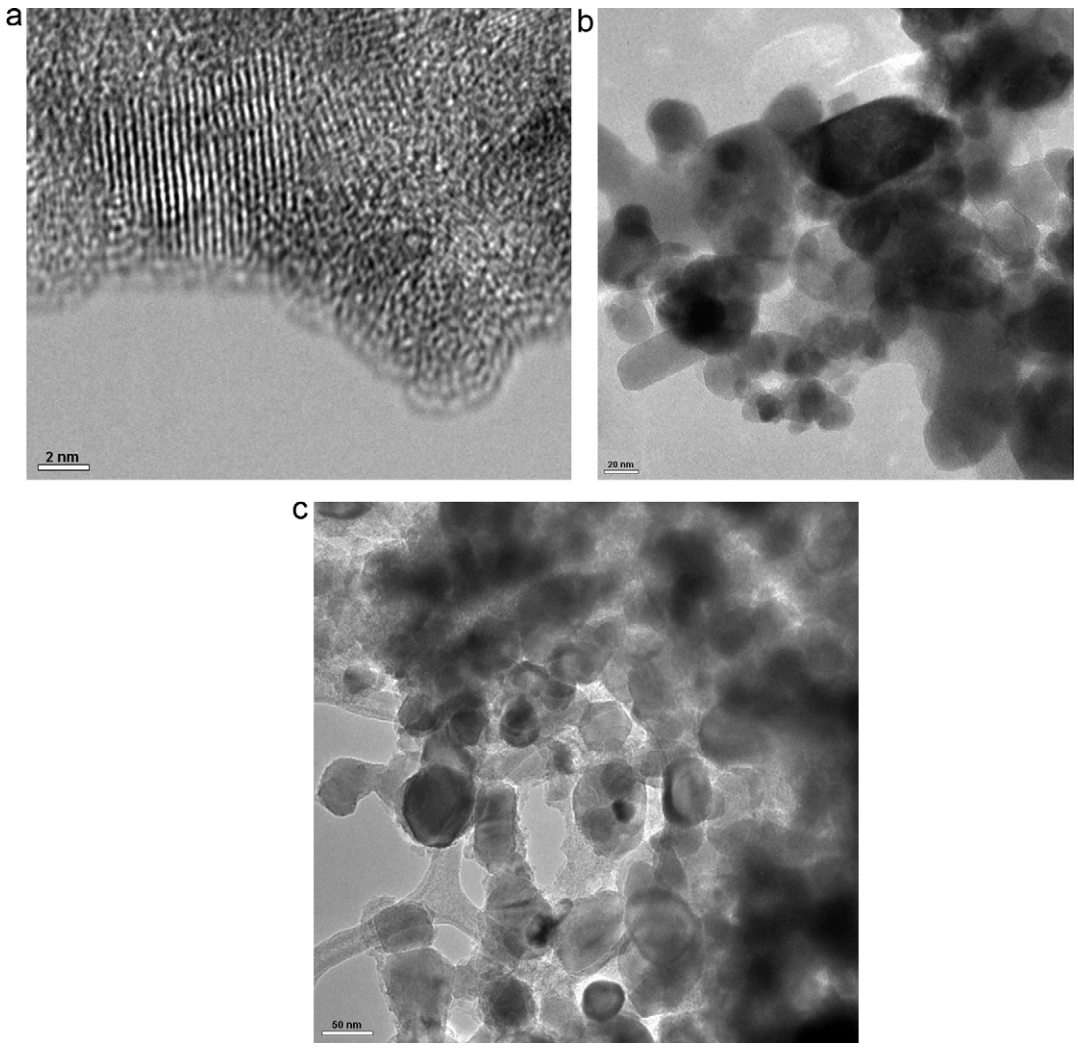

Fig. 4. TEM images of (a) only TiO_2, (b) only ZnO, and (c) TiO_2–ZnO hybrid samples.

samples) and the exposure time was in minutes (a few to tens of minutes). For each photoactivation process at a particular wavelength, we kept the total number of incident photons to activate the photochemical reaction per unit area ([power to enable the photochemical reaction × time]/[spot size × photon energy]) constant (at 10^{22} m^{-2}). We experimentally investigated optical spectral photocatalytic recovery behavior (i.e., optical degradation obtained by photocatalysis reactions) of these nanocomposite films as a function of the excitation wavelengths (from 310 nm to 469 nm) in the UV and visible ranges. We optically measured these photocatalytic recovery levels using transmission spectroscopy in the visible spectral range after exposure at each of the selected activation wavelengths. In these experimental characterizations, we calculated the optical degradation level as the percentage ratio of the area between the transmittance spectra before and after photocatalytic degradation to the area between those before and after addition of methylene blue as given in (1). Here $T_{clean}(\lambda)$ is the transmittance level of the sample across the visible part of the spectrum when it is clean (before contamination with methylene blue), $T_{contanimated}(\lambda)$ is that of the sample when it is contaminated with methylene blue (before optical activation), and $T_{activated}(\lambda)$ is that of the sample when it is optically activated at a particular excitation wavelength. The optical recovery characterization showed the amount of the adsorbed contaminant that was photocatalytically degraded at a particular activation wavelength.

$$\text{Optical degradation percent} = \frac{\int [T_{activated}(\lambda) - T_{contaminated}(\lambda)]d\lambda}{\int [T_{clean}(\lambda) - T_{contaminated}(\lambda)]d\lambda} \times 100 \quad (1)$$

As shown in Figs. 5 and 6, we measure the transmittance spectra of $T_{clean}(\lambda)$, $T_{contanimated}(\lambda)$, and $T_{activated}(\lambda)$ for the composite films embedded with nanoparticles in different combinations: TiO_2–ZnO nanocomposite in (a), only TiO_2 in (b), and only ZnO in (c), as well as the control group of acrylic host resin without any nanoparticles in (d), at two different activation wavelengths (activated at 330 nm in Figs. 5a–d and 403 nm in Fig. 6a–d). Here we observe a significant decrease in the optical transmittance of all of these films as they are contaminated with methylene blue. Except for the control group, this is followed by a subsequent increase in the transmittance after the film is photocatalytically activated using a monochromatic light at the particular excitation wavelength. The decreased transmittance in the visible range substantially recovers its original level during the photoactivation process if there is sufficient photocatalytic activity. For the negative control groups (in Figs. 5d and 6d), when we monitor the optical activity that takes place in the host (resin) film with no particle, we observe

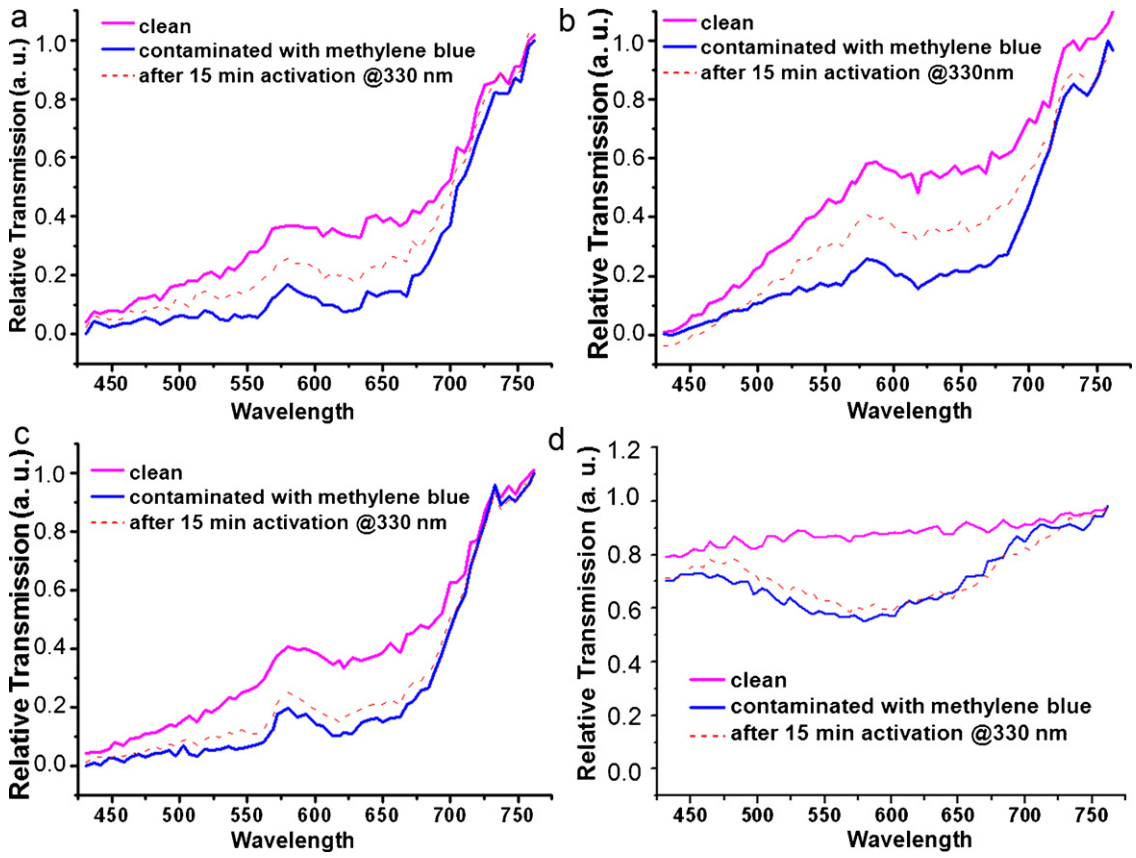

Fig. 5. Optical transmission of the nanocomposite films consisting of (a) TiO_2–ZnO combined nanoparticles, (b) only TiO_2 nanoparticles, (c) only ZnO nanoparticles, and (d) those of the negative control group that contains only host resin (without any nanoparticles) before and after being contaminated with methylene blue, and after being activated at an optical wavelength of 330 nm, while keeping the total number of incident photons to activate the photochemical reaction per unit area ([power to enable the photochemical reaction × time]/[spot size × photon energy] constant at 10^{22} m^{-2}.

clearly much weaker degradation of methylene blue at the excitation wavelength compared to those of the samples that contain nanoparticles. Here we do not observe any significant effect of photolysis because of low level of optical excitation power used in our study (although direct photolysis can possibly occur in general in addition to the photocatalytic process if the ultraviolet radiation exceeds a certain level of energy [31]). Also, oxidation of molecular oxygen can only possibly be observed at high optical intensities. In our case, the excitation radiation intensities are very low for a noteworthy contribution from the oxidation of molecular oxygen [32]. This implies that the observed optical activity in Figs. 5a–c and 6a–c is primarily a result of the photocatalysis, if any, but not of the photolysis, for the operating power levels adopted in our experimental characterizations. For optical excitation at 330 nm in Fig. 5, we find out that TiO_2 nanoparticles have the highest photocatalytic activity, while ZnO nanoparticles exhibit weaker photocatalytic activity. In the literature, ZnO is considered as a good alternative for TiO_2 [33]; in our case, the size effect can be one of the factors to decrease their corresponding photocatalytic activity. For optical excitation at 403 nm in Fig. 6, we find out that the combination of TiO_2–ZnO nanoparticles have the highest photocatalytic activity, while the others exhibit weaker photocatalytic activity.

To develop a better understanding of the synergistic effect, Fig. 7 depicts a complete set of the photocatalysis experiments, spectrally resolved at different excitation wavelengths tuned from 310 nm to 469 nm. These optical degradation levels were obtained using (1) with photochemical reactions enabled, all at a constant total number of incident photons per unit area, but at different photochemical reaction wavelengths (activation wavelengths). As a result of these experiments, we observe that TiO_2 shows higher optical spectral photocatalytic degradation than zinc oxide for all activation wavelengths as presented in Fig. 7. The fast decrease in the optical degradation is observed at a shorter wavelength (~370 nm) for TiO_2 than for ZnO (~380 nm) as seen in Fig. 7. This different photocatalytic behavior is related to the absorption band edges of the incorporated nanoparticles. Both TiO_2 (in anatase form) and ZnO (zincite) have bandgap energies of about 3.3 eV, corresponding to an optical wavelength of ~376 nm confirmed by the XRD phase identification studies. The difference in the absorption edge is attributed to the widening of the bandgap with the shrinking size of TiO_2 and ZnO nanoparticles in this work. TiO_2 continues its photocatalytic activity at significant levels when optically activated at wavelengths between 380 nm and 420 nm as observed in Fig. 7. This is due to the absorption tail of anatase TiO_2. Indirect transitions are allowed at these activation wavelengths. On the other hand as shown in Fig. 7, TiO_2–ZnO nanocomposite films exhibit enhanced photocatalytic activity in the near-UV range and some part of the visible spectrum (up to 469 nm), which is a part of the solar spectrum more abundant in daylight compared to deep UV range. In Fig. 7, the optical recovery (degradation) level of TiO_2–ZnO nanocomposite is 30% at 400 nm activation wavelength when TiO_2 alone has only 14% and ZnO alone has only 3%. Also at longer wavelengths TiO_2–ZnO nanocomposite film further continues its photocatalytic activity, while TiO_2 alone or ZnO alone does not exhibit any significant photocatalytic activity beyond 400 nm. For TiO_2–ZnO nanocomposite films, though, even at 440 nm activation wavelength, an optical degradation of 20% is achieved.

Fig. 8 exhibits our experimental data for optical wavelengths longer than 380 nm where the rates of degradation tend to decrease; these results clearly demonstrate the photocatalytic

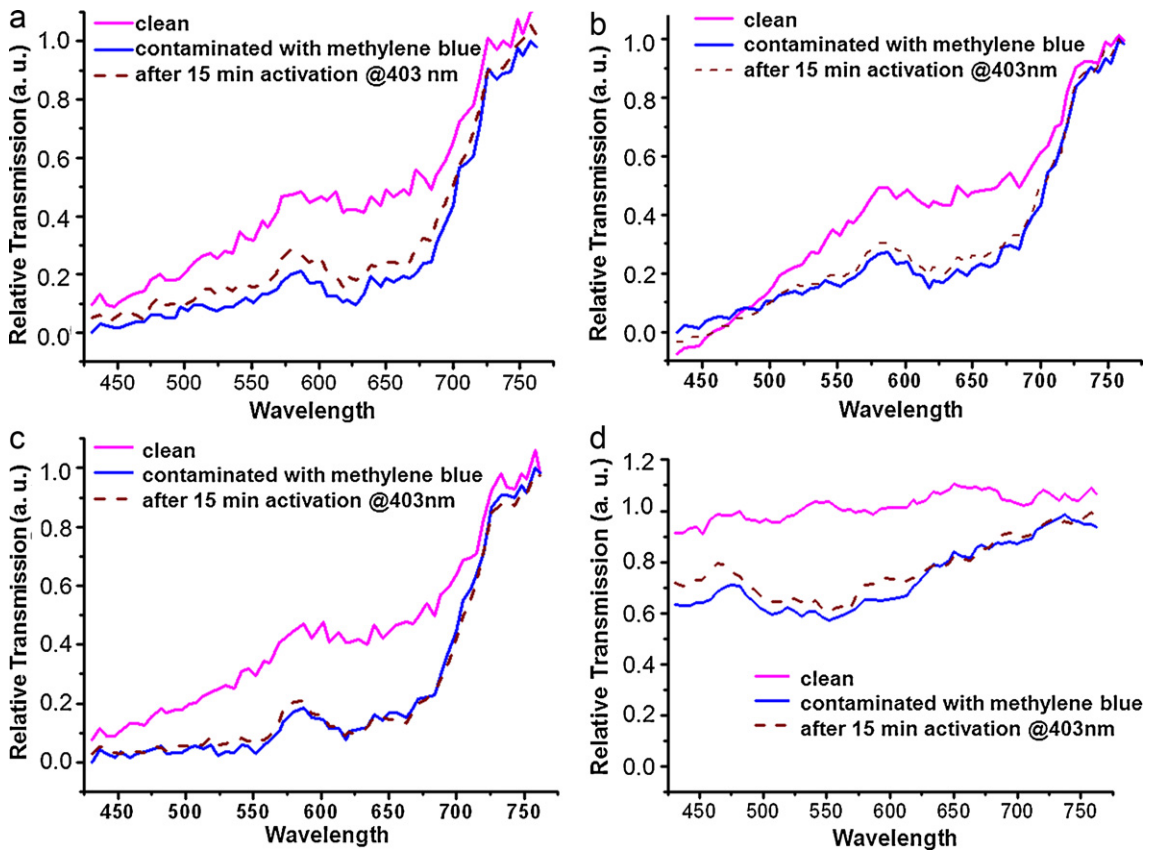

Fig. 6. Optical transmission of the nanocomposite films consisting of (a) TiO_2–ZnO combined nanoparticles, (b) only TiO_2 particles, and (c) ZnO nanoparticles before and after contaminated with methylene blue, and after photocatalytically activated at 403 nm with a constant total number of incident activation photons per unit area (10^{22} m^{-2}) along with (d) those of the control group (host resin without any nanoparticles).

enhancement in TiO_2–ZnO nanocomposite film in the near UV and visible spectral range. We observe that TiO_2–ZnO combination has an enhanced optical degradation where only TiO_2, only ZnO, or control groups have no significant activity. The underlying mechanism of the increased photocatalytic activity in TiO_2–ZnO composites in comparison to the individual metal oxides is attributed to charge transfer. In the case of TiO_2–ZnO composites it is possible to facilitate the use of the indirect bandgap of TiO_2, which has a narrower gap than the direct one, along with subsequent charge transfer of the exited electrons to ZnO, whose conduction band energetically matches, as confirmed by the phase identification (obtained by XRD results). The modification in TiO_2 bandgap (from 3.2 eV to 3.3 eV) due to quantum size effect is also taken into account for the TiO_2 nanoparticles [34]. The suggested charge transfer in TiO_2–ZnO composites then possibly enhances the photocatalytic activity even when the incident photon energy level is lower than the bandgap of TiO_2. The increased photocatalytic activity can be explained with the decreased recombination rate as the electrons are transferred from the conduction band of TiO_2 to the conduction

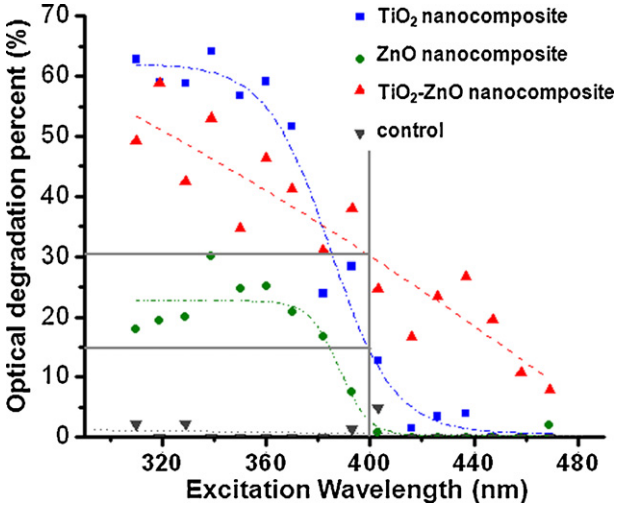

Fig. 7. Spectral photocatalytic behavior for optically activating photochemical reactions at different excitation wavelengths tuned from 310 nm to 469 nm.

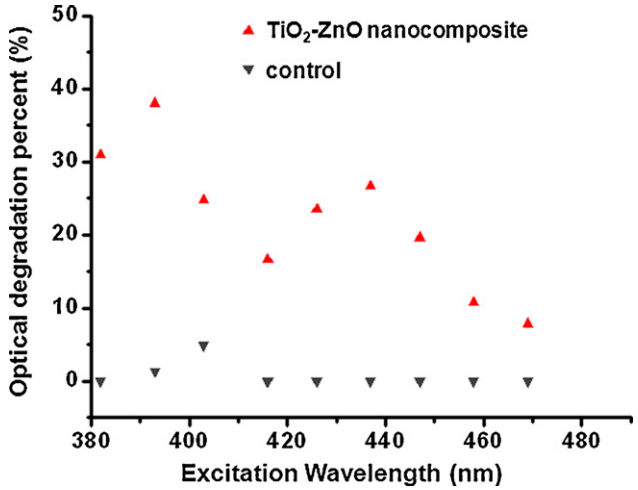

Fig. 8. Photocatalytic degradation in the spectral range of 380–469 nm.

band of ZnO while the holes are transferred from the valance band of ZnO to the valance band of TiO_2. Previous research reports also correlate higher photocatalytic efficiency with the charge transfer [12–14,16]. Also improved photocatalytic activity in ZnO–TiO_2 nanocomposites can also stem from the high binding energy of ZnO and enhanced reactivity of TiO_2, which increases the process of electron and hole transfer between the respective conduction and valence bands.

In addition to these results, we performed extensive characterization to optimize the mass percentages for obtaining high photocatalytic efficiencies at different wavelengths. The set of samples with the mass percentages leading to the best results are presented here. In the case of lower mass percentages of nanoparticles, the photocatalytic activity is expectedly weaker and clearly suboptimal due to insufficient number of embedded nanoparticles in the film. For the cases of higher mass percentages, we observe that, although the overall photocatalytic efficiency enhancement is relatively lower due to agglomeration of nanoparticles, the photocatalytic synergy still enhances comparatively the optical recovery behavior towards the visible range. In this co-integration approach, we thus repeatedly observe in our samples to different extends that the level of photocatalytic degradation can be increased for optical activation in the near-UV and visible spectra of light.

4. Conclusions

In conclusion, we formed highly active photocatalytic films with immobilized TiO_2–ZnO nanoparticles that were integrated inside three-dimensional acrylic sol–gel. For a comparative study, we used three different samples including only TiO_2 (~6 nm in diameter), only ZnO (~40 nm in diameter) and TiO_2–ZnO combined nanocomposites. By integrating TiO_2 and ZnO nanoparticles in the acrylic host resin, we achieved a good dispersion of the nanoparticles compared to simply blending them mechanically into the host. SEM pictures verify the porous surface structure of the composite thin films, which resulted in comparatively larger photodegradation area and photocatalytic activity. We observed that although both of the nanoparticles had similar photocatalytic properties, TiO_2 nanoparticles provided much better photocatalytic activity than ZnO nanoparticles for all photochemical reaction wavelengths. On the other hand, even though TiO_2 embedded films demonstrated higher photocatalytic efficiency in the deeper UV ranges, the co-integration of TiO_2 and ZnO nanoparticles into the same resin substantially improved the photocatalytic activity in the near-UV and visible spectral ranges, where the intrinsic photocatalytic activities of TiO_2 and ZnO nanoparticles individually were found to be considerably weak. Particularly for the excitation wavelengths of photochemical reactions longer than 400 nm, where the negative control group and ZnO nanoparticles alone yield no observable photodegradation level and TiO_2 nanoparticles alone lead to a low photodegradation level of 14%, the synergic combination of TiO_2–ZnO nanoparticles achieves a photodegradation level as high as 30%. This proof-of-principle spectrally resolved activation demonstration shows great promise of these hybrid nanocomposites particularly for photocatalytic degradation in outdoor applications using near-UV and visible spectral ranges of the solar spectrum. As we demonstrated the synergistic effect of the photocatalytic TiO_2–ZnO hybrid nanocomposites in the near-UV and visible spectral ranges by the optical characterizations, we exhibited the evidences of the nanostructure, crystallography, and chemical bonding states for the films through different material characterization techniques including EDS, SEM, HRTEM and XRD. The lattice images of the hybrid nanoparticles by HRTEM and the phase identification by the XRD patterns showed that there is no chemical bonding between the two different nanoparticles. Hence the enhanced photocatalytic activity is attributed to the transfer of electrons from the conduction band of TiO_2 to that of ZnO and the holes from the valance band of ZnO to that of TiO_2, which decreases the recombination rate of these photogenerated electron–hole pairs.

Hybrid nanocomposite coatings with enhanced activity in the visible range can be used for all internal–external metal, glass, ceramic and wood surfaces. With their distinctive properties such as photocatalytic self-cleaning, resistance towards bacteria and elimination of various air pollutants, they can be applied to large-area surfaces in the form of paint, coating, cement additives and so on. Such functional surfaces offer strong potential for use in various emerging fields in the energy, construction, automotive, health, security and other industrial sectors. Thin film coating on large areas is low cost and simple when using the presented sol–gel method. Among these different applications, large-area applications that offer solutions to combat environmental pollution and to prevent wide-scale accumulation of unwanted contaminants receive industrial attention for their enhanced self-cleaning properties under sunlight.

Acknowledgements

This work is supported by EU-N4E NoE 248855 and TUBITAK under the Project Nos. 110E010, 109E004, 109E002, and 107E088. Also, HVD acknowledges additional support from the Turkish Academy of Sciences (TUBA) Distinguished Young Scientist Award (GEBIP) and European Science Foundation (ESF) European Young Investigator Award (EURYI) Programs, and EM and IMS acknowledge TUBITAK Graduate Fellowships. The authors are pleased to acknowledge Prof. M. Ozenbas for fruitful discussions with him.

References

[1] J.S. Dalton, P.A. Janes, N.G. Jones, J.A. Nicholson, K.R. Hallam, G.C. Allen, Environ. Pollut. 120 (2002) 415–422.
[2] S. Banerjee, J. Gopal, P. Muraleedharan, A.K. Tyagi, B. Raj, Curr. Sci. 90 (2006) 1378–1383.
[3] T. Sato, K. Masaki, K. Sato, Y. Fujishiro, A. Okuwaki, J. Chem. Technol. Biotechnol. 67 (1996) 339–344.
[4] J.A. Navio, F.J. Marchena, M. Roncel, M.A. Del la Rosa, J. Photochem. Photobiol. A: Chem. 55 (1991) 319–322.
[5] R. Asahi, T. Morikawa, T. Ohwaki, K. Aoki, Y. Taga, Science 293 (2001) 269–271.
[6] S. In, A. Orlov, R. Berg, F. Garcia, S. Pedrosa-Jimenez, M.S. Tikhov, D.S. Wright, R.M. Lambert, J. Am. Chem. Soc. 129 (2007) 13790–13791.
[7] S. Sakthivel, H. Kisch, Angew. Chem. Int. Ed. 42 (2003) 4908–4911.
[8] G. Liu, L. Wang, H.G. Yang, H.M. Cheng, G.Q. Lu, J. Mater. Chem. 20 (2010) 831–843.
[9] M. Long, W.M. Cai, J. Cai, B.X. Zhou, X.Y. Chai, Y.H. Wu, J. Phys. Chem. B 110 (2006) 20211–20216.
[10] M.K.I. Senevirathna, P.K.D.D.P. Pitigala, K. Tennakone, J. Photochem. Photobiol. A 171 (2005) 257–259.
[11] K. Sayama, R. Yoshida, H. Kusama, K. Okabe, Y. Abe, H. Arakawa, Chem. Phys. Lett. 277 (1997) 387–390.
[12] Z. Zhang, Y. Yuan, Y. Fang, L. Liang, H. Ding, L. Jin, Talanta 73 (2007) 523–528.
[13] G. Marci, V. Augugliaro, M.J. Lopez-Munoz, C. Martin, L. Palmisano, V. Rives, M. Schiavello, R.J.D. Tilley, A.M. Venezia, J. Phys. Chem. B 105 (2001) 1033–1040.
[14] S. Janitabar-Darzi, A.R. Mahjoub, J. Alloy Compd. 486 (2009) 805–808.
[15] H.Y. Yang, S.F. Yu, S.P. Lau, X. Zhang, D.D. Sun, G. Jun, Small 5 (20) (2009) 2260–2264.
[16] D. Barreca, E. Comini, A.P. Ferrucci, A. Gasparotto, C. Maccato, C. Maragno, G. Sberveglieri, E. Tondello, Chem. Mater. 19 (2007) 5642–5649.
[17] R. Comparelli, P.D. Cozzoli, M.L. Curri, A. Agostiano, G. Mascolo, G. Lovecchio, Water Sci. Technol. 49 (2004) 183–188.
[18] G. Mascolo, R. Comparelli, M.L. Curri, G. Lovecchio, A. Lopez, A. Agostiano, J. Hazard. Mater. 142 (2007) 130–137.
[19] I.M. Soganci, E. Mutlugun, S. Tek, H.V. Demir, D. Yucel, G. Celiker, Proc. LEOS (2006) 549–550.
[20] G. Celiker, D. Yucel, E. Mutlugun, I.M. Soganci, S. Tek, H.V. Demir, Proc. PRA World 2nd Int. Nano Hybrid Coat. Conf. 'Developments of the Minute' (PRA 2007), Brussels, Belgium, 2007.
[21] S. Tek, H.V. Demir, D. Yucel, G. Celiker, The 7th Pacific Rim Conf. on Lasers and Electro-Optics (CLEO Pacific Rim 2007), Seoul, Korea, 2007.
[22] S. Tek, E. Mutlugun, I.M. Soganci, N.K. Perkgoz, D. Yucel, G. Celiker, H.V. Demir, J. Nanophoton. 1 (2007).

[23] A. Rachel, M. Subrahmanyam, P. Boule, Appl. Catal. B: Environ. 37 (2002) 301–308.
[24] I.M. Arabatzis, S. Antonaraki, T. Stergiopoulos, A. Hiskia, E. Papaconstantinou, M.C. Bernard, P. Falaras, J. Photochem. Photobiol. A: Chem. 149 (2002) 237–245.
[25] H.D. Jang, S.K. Kim, S.J. Kim, J. Nanoparticle Res. 3 (2001) 141–147.
[26] C.H. Xue, S.T. Jia, H.Z. Chen, M. Wang, Sci. Technol. Adv. Mater. 9 (2008) 1–5, 035001.
[27] Z. Yuan, L. Zhang, J. Mater. Chem. 11 (2001) 1265–1268.
[28] T. Deguchi, K. Imai, M. Iwasaki, H. Tada, S. Ito, J. Electrochem. Soc. 147 (2000) 2263–2267.
[29] S.H. Lee, S. Pumprueg, B. Moudgil, W. Sigmund, Colloid Surf. B: Biointerfaces 40 (2005) 93–98.
[30] T. Tatsuma, S. Tachibana, T. Miwa, D.A. Tryk, A. Fujishima, J. Phys. Chem. B 103 (1999) 8033–8035.
[31] P.V. Kamat, Chem. Rev. 93 (1993) 267–300.
[32] T. Zhang, T. Oyama, H.S. orikoshi, J. Zhao, N. Serpone, H. Hidaka, Sol. Energy Mater. Sol. Cells 73 (2002) 287–303.
[33] S. Chakrabarti, B.K. Dutta P, J. Hazard. Mater. B112 (2004) 269–278.
[34] H.S. Lee, C.S. Woo, B.K. Youn, S.Y. Kim, S.T. Oh, Y.E. Sung, H.-I. Lee, B Top. Catal. 35 (2005) 255–260.